Nanosecond Time-Resolved Infrared Spectroscopy Distinguishes Two K Species in the Bacteriorhodopsin Photocycle

Jun Sasaki,* Tetsuro Yuzawa,‡ Hideki Kandori,* Akio Maeda,* and Hiro-o Hamaguchi‡

*Department of Biophysics, Faculty of Science, Kyoto University, Kyoto 606-01, Japan, and ‡Kanagawa Academy of Science and Technology (KAST), Sakato 100-1, Takatsu-ku, Kawasaki-shi, Kanagawa 213, Japan

ABSTRACT The photochemical reaction process of bacteriorhodopsin in the nanosecond time range (−120~860 ns) was measured in the 1400~900 cm^{-1} region with an improved time resolved dispersive-type infrared spectrometer. The system is equipped with a newly developed detection unit whose instrumental response to a 5-ns laser pulse has a full width of the half-maximum of 60 ns. It provides highly accurate data that enabled us to extract a kinetic process one order of magnitude faster than the instrumental response. The spectral changes in the 1400~900 cm^{-1} region were analyzed by singular value decomposition and resolved into three components. These components were separated by fitting with 10- and 1000-ns exponential functions and a step function, which were convoluted with the instrumental response function. The components with decay time constants of 10 and 1000 ns are named K and KL, respectively, on the basis of previous visible spectroscopy. The spectral shapes of K and KL are distinguishable by their hydrogen-out-of-plane (HOOP) modes, at 958 and 984 cm^{-1}, respectively. The former corresponds to the K intermediate recorded at 77 K and the latter to a K-like photoproduct at 135 K. On the basis of published data, these bands are assigned to the 15-HOOP mode, indicating that the K and KL differ in a twist around the C_{14}-C_{15} bond.

INTRODUCTION

Bacteriorhodopsin is a retinal protein that functions as a light-driven proton pump in *Halobacterium salinarium*. The retinal chromophore is covalently bound to Lys-216 through a protonated Schiff base; its configuration in the light-adapted bacteriorhodopsin (BR) is all-*trans*. Light absorption by the all-*trans* chromophore triggers a cyclic reaction that is comprised of a series of intermediates named J, K, KL, L, M, N, and O (Mathies et al., 1991; Lanyi, 1993).

These intermediates are distinguished by spectral changes in the visible region, as measured by time-resolved measurements at room temperature and by static measurements upon stabilizing intermediates at low temperatures. In general, these intermediates are placed into sequence in the order of their appearance, or the increasing temperatures at which they are stable.

The early photoproducts J, K, and KL, which exhibit red-shifted absorption maxima relative to BR, have been distinguished by time-resolved measurement. The first step of the cycle, J formation, occurs with the photochemical isomerization of the all-*trans* retinal chromophore to the 13-*cis* form in the subpicosecond time range (Dobler et al., 1988; Mathies et al., 1988; Kandori et al., 1993). The J-to-K conversion occurs in 3 ps with a slight blue-shift of the absorption spectrum. This was explained as vibrational cooling (Doig et al., 1991). A further small blue-shift of the spectrum was observed in the nanosecond time range and was named the K-to-KL conversion (Shichida et al., 1983; Milder and Kliger, 1988). Resonance Raman spectroscopy by Doig et al. (1991) also distinguished between the spectra at 3 ps and 3.7 ns, which were attributed to K and KL, respectively. The difference between them was mainly in the hydrogen-out-of-plane (HOOP) modes, whose intensities were larger in KL than in K.

Visible spectroscopy at liquid N_2 temperature also detected a red-shifted intermediate and was called K (Stoeckenius and Lozier, 1974; Lozier et al., 1975; Tokunaga et al., 1976). This intermediate has not yet been assigned to either K or KL. Infrared spectroscopy, however, discriminated two kinds of K intermediates at low temperature; one is the K produced by irradiation of BR at 77 K (K^{LT}) (Rothschild and Marrero, 1982; Siebert and Mäntele, 1983), and the other is produced by irradiation of BR at 135 K as a mixture with K^{LT} (Rothschild et al., 1985). A significant difference between them was found in the HOOP region.

Subsequently, time-resolved measurements by infrared spectroscopy in submicrosecond region (Sasaki et al., 1993; Weidlich and Siebert, 1993) revealed the spectrum of an intermediate that corresponds to KL. It more closely resembles the K-like intermediate at 135 K than K^{LT} (Sasaki et al., 1993). Therefore, it was suggested that the K-to-KL conversion, which corresponds to the change between K^{LT} and the K-like intermediate at 135 K, would take place in the early nanosecond domain. However, time-resolved infrared spectroscopy covering an early nanosecond domain was not

Received for publication 12 December 1994 and in final form 24 February 1995.

Address reprint requests to Dr. Akio Maeda, Department of Biophysics, Faculty of Science, Kyoto University, Kitashirawaka-Oiwake-cho, Sakyo-Ku, Kyoto 606-01, Japan. Tel.: 81-75-753-4210; Fax: 81-75-753-4210; E-mail: kandori@photo2.biophys.kyoto-u.ac.jp.

Abbreviations used: BR, light-adapted bacteriorhodopsin; HOOP, hydrogen-out-of-plane; K^{LT}, K intermediate produced by irradiation at 77 K; SVD, singular value decomposition; IRF, instrumental response function; FWHM, full width at half-maximum.

0006-3495/95/05/2073/08 $2.00

available except for the picosecond infrared spectroscopy by Diller et al. (1992) which, however, did not cover the HOOP region.

In the present study, we applied a recently developed nanosecond time-resolved infrared spectroscopic system that has a time resolution of about 60 ns and covers the 1400~900 cm^{-1} region. The analysis of the spectra by use of singular value decomposition (SVD) and the correction of the kinetic profiles with a measured instrumental response function (IRF) enabled us to resolve two different K species (K and KL), which decay in 10 and 1000 ns, respectively. The spectral shapes of K and KL resemble those of K^{LT} and the K-like intermediates at 135 K, respectively.

MATERIALS AND METHODS

Bacteriorhodopsin in the purple membrane was prepared by the standard method (Oesterhelt and Stoeckenius, 1974). The membrane suspensions in water were then dried on a BaF_2 window (16 mm in diameter) in room air. The dried bacteriorhodopsin was covered with 1 μl of water and sealed with the second window. Water evaporation was prevented during the recording for at least 6 h by sealing with grease. This set was mounted into a copper block. The sample was light-adapted by exposure to laser beam before recording.

A nanosecond time-resolved dispersive-type infrared spectroscopic system (Yuzawa et al., 1994) was used for the present measurements. The BR film was excited by the second harmonic (532 nm) of a cw Q-switch Nd:YLF laser (Spectra Physics, TFR, 5-ns pulse width, 49 Hz, Mountain View, CA). The beam was loosely focused on a circle of ~2 mm in diameter. The excitation energy was 70 μJ/pulse. Below this energy level, decrease in the absorbance at 1200 cm^{-1} (C—C stretching vibration of BR) upon excitation was in proportion to the excitation energy.

The detection system is based on that for the previous experiment (Sasaki et al., 1993) but is much improved for the time-resolution (Yuzawa et al., 1994). The monitoring light source for the measurement of the IR spectrum was $MoSi_2$ (JASCO, Tokyo, Japan). After passing through the sample, light was dispersed with a Hitachi I-3000 grating infrared spectrometer and was focused on a photovoltaic MCT detector (Kolmar Technologies, Inc. KV103-1-A-1-SMA, Concord, MA). Only the intensity changes by the photoreaction of the sample were extracted by an AC-coupled amplifier, and they were recorded on a digital oscilloscope (Tektronix, DSA 602, 11A4, Portland, OR).

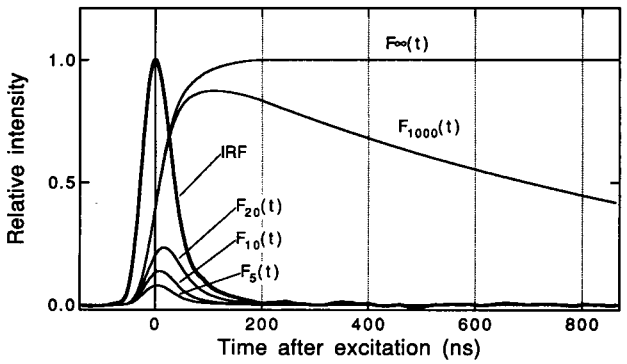

FIGURE 1 IRF (**bold line**) and the kinetic profiles obtained by convolution of exponential decays with IRF. IRF was obtained by recording response of MCT detector to 5-ns laser pulse. Exponential functions with time constant of 5, 10, 20, and 1000 ns and step function were convoluted with the IRF as described in the text (denoted as $F_5(t)$, $F_{10}(t)$, $F_{20}(t)$, $F_{1000}(t)$, and $F_\infty(t)$, respectively).

Intensity changes from −120 to 860 ns at every 2 ns were recorded at each fixed wavenumber 1024 times. Because systematic wave-like noise was generated by the laser in the nanosecond time domain, the measurements were done both in the absence and presence of the shutter inserted between the laser and the sample. The signals were obtained by subtracting the contribution of the noise determined as the intensity changes in the presence of the shutter. The wavenumbers for the measurements were varied from 1400 to 900 cm^{-1} at every 2 cm^{-1} (8 cm^{-1} in spectral resolution). The extent of photoreaction was monitored at 1200 cm^{-1} after each scan and was confirmed to be unchanged from that before the scan. This rules out the possibility of the irreversible photochemical reaction when BR is exposed to repeated laser pulses with intensities above 10 mJ/cm^2 (Govindjee et al., 1990). The whole scan process took about 3 h and was repeated 8 times.

The IRF (instrumental response function) of the present apparatus under our experimental conditions was obtained by detecting the scattered light of the laser pulse with the MCT detector (Fig. 1). The recording of the kinetic trace was repeated 1024 times for averaging. The IRF exhibits the full width at the half-maximum (FWHM) of 60 ns with a slightly asymmetric curve toward the decay side. The time for the maximal IRF was regarded as time 0. For the kinetic analysis whose time constant is comparable with the IRF, we calculated the corrected decay curve, $F_T(t)$, by convolution with the present IRF as follows:

$$F_T(t) = \int_{-\infty}^{t} \exp(-(t - t')/T \cdot \mathrm{IRF}(t')dt', \quad (1)$$

where T represents the decay time constant. In Fig. 1, we show several curves that are used for the fitting below. The instantaneous system rise (denoted "step function") is also calculated by the following equation:

$$\text{step function} = F_\infty(t) = \int_{-\infty}^{t} \mathrm{IRF}(t')dt'. \quad (2)$$

Singular value decomposition (SVD) was performed with a program SPSERV purchased from Dr. Csaba Bagyinka (Biological Research Center of the Hungarian Academy of Science, Szeged, Hungary).

RESULTS

Infrared spectral changes from −120 to 860 ns after the excitation of BR were recorded at every 2 ns in the 1400~900 cm^{-1} region at every 2 cm^{-1}. We did not record the region between 1500 and 1700 cm^{-1}, where the sample has strong absorption bands, because lower sensitivity of the detector than the one used previously (Sasaki et al., 1993) did not afford reliable results in this region. The complete data set is composed of 251×501 points along the wavenumber and time axes. Every 10 data points along the time axis were averaged to reduce the data to 251×50 points to make the data size suited for SVD calculations in our personal computer.

Fig. 2 shows a series of spectral changes (50 spectra from −120 to 860 ns with a 20-ns interval) after the excitation of BR. There are three notable changes in the difference spectra: 1) a rise in the −20 to 80 ns time domain (clearly observed in 1300~1100 cm^{-1}); 2) a gradual decay of the whole signals after 100 ns; and 3) a change in the spectral shape in the 1000~950 cm^{-1} region. The first signal is mainly due to the system response, because the time scale (−20~80 ns) is comparable with the present IRF (Fig. 1). The gradual decay after 100 ns, the second change, corresponds to the KL-to-L transition of 1 μs, which was detected by infrared (Sasaki et al., 1993) and also visible spectroscopy (Váró and Lanyi, 1991).

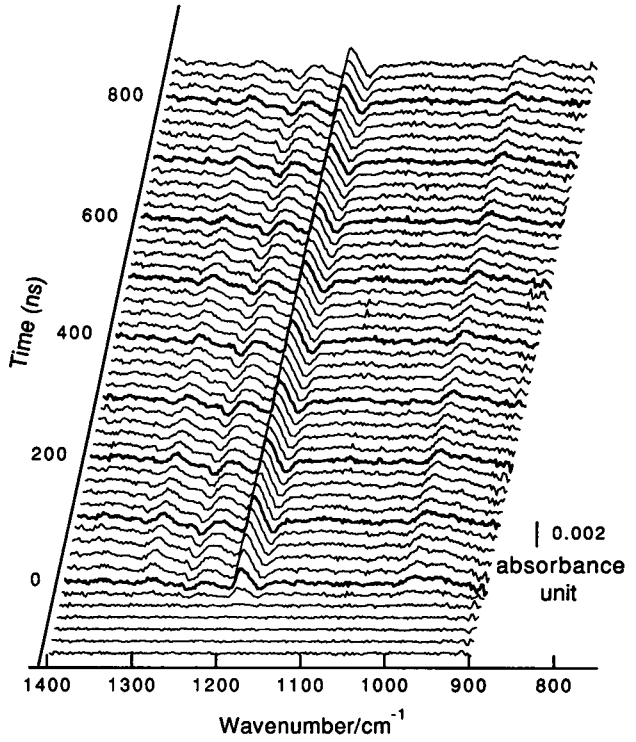

FIGURE 2 The infrared spectral changes of BR in the −120~860-ns time domain after the excitation with laser of 532 nm and 5-ns pulse width. The spectral resolution is 8 cm^{-1} with the data point at every 2 cm^{-1} in the 1400~900 cm^{-1} region. The spectra depicted by bold lines are the recordings at 0, 200, 400, 600, and 800 ns.

The third is the change in the ratio of the intensities of the 960 cm^{-1} band to the 984 cm^{-1} band. The ratio is nearly equal in the early time domain (20–80 ns) and decreases later, in agreement with the previous results by Sasaki et al. (1993). Similar time-dependent changes are seen in the spectra averaged in a wider time range presented by Yuzawa et al. (1994).

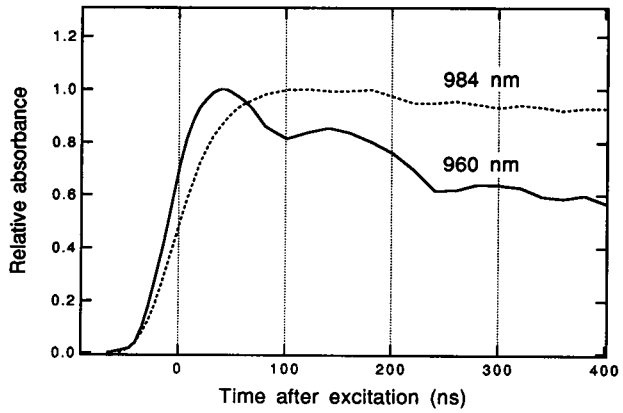

FIGURE 3 Normalized kinetic traces of the bands at 960 and 984 cm^{-1}. These traces are the plots of the data in Fig. 2 at 960 and 984 cm^{-1}, and drawn with solid and dashed line, respectively. The original amplitude of the maxima of the kinetic traces at 960 and 984 cm^{-1} are 5.96×10^{-4} and 1.01×10^{-3} absorbance units, respectively.

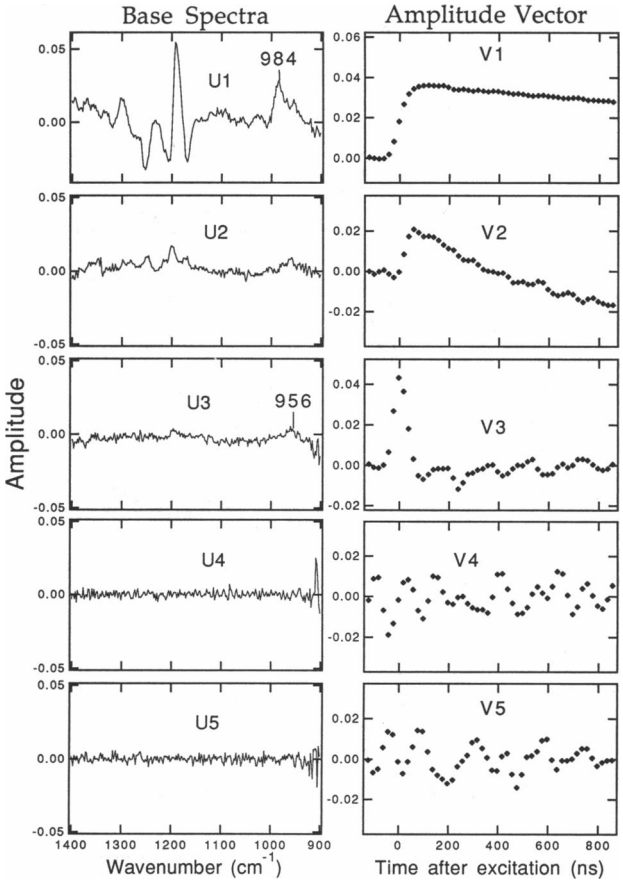

FIGURE 4 The first five base spectra (U) and the amplitude vectors (V) obtained by SVD analysis on the spectra in Fig. 2. Each Ui and Vi are shown by multiplying with a square root of each weight factor, Si. The first three of the U spectra and V vectors are regarded as the changes beyond noise level, whereas the others are regarded as only noise.

These observations are more clearly seen by comparing the kinetic curves at 984 and 960 cm^{-1} as shown in Fig. 3. The band at 960 cm^{-1} rises and decays more rapidly after excitation than does the 984 cm^{-1} band, as was expected from the change in the ratio between the two bands. These kinetic curves demonstrate that more than one decaying component exists after excitation in the nanosecond time domain and that the 960 cm^{-1} band is contributed by a rapidly changing component more than the 984 cm^{-1} band.

To analyze the data in Fig. 2 in more detail, we applied singular value decomposition (SVD) analysis to a matrix with 251×50 data points (A). This procedure converted these data to a linear combination of 50 products of base spectra (U), weight factors (S), and amplitude vectors (V) as follows:

$$A = \Sigma Ui \times Si \times Vi \; (i = 1 \sim 50) \qquad (3)$$

The first five sets of the U spectra and V vectors, which were multiplied by the square root of respective weight factors, are presented in Fig. 4. Among them, the first three show signals exceeding the noise level, whereas U4 and U5 appear to be only random noise. Some systematic wave-like signal in V4 and V5 should also be regarded as noise from the laser

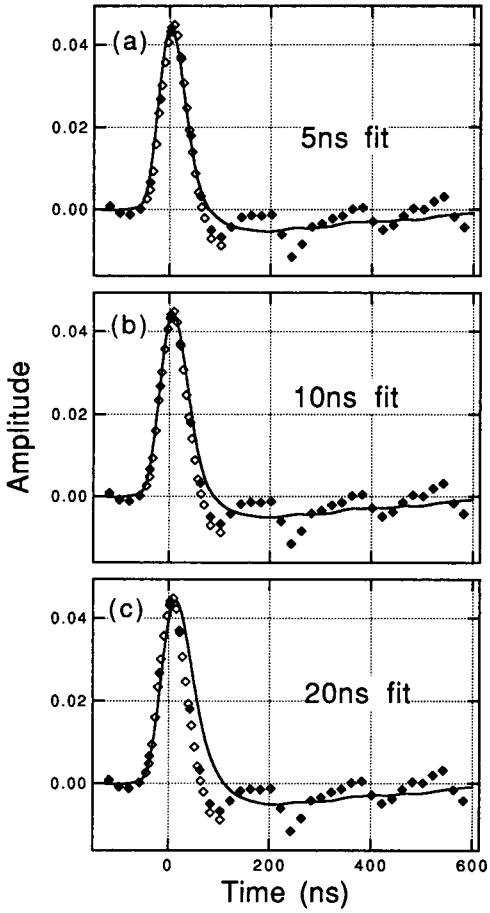

FIGURE 5 The best fit of V3 (■) with a combination of $F_\infty(t)$, $F_{1000}(t)$, and $F_5(t)$ (*a*), $F_{10}(t)$ (*b*), or $F_{20}(t)$ (*c*) (——). V3 could be almost approximated by use of $F_5(t)$ or $F_{10}(t)$ but noticeably deviated with $F_{20}(t)$. Open squares also represents V3 with more data points around time 0 derived from SVD of increased spectral number by decreasing average.

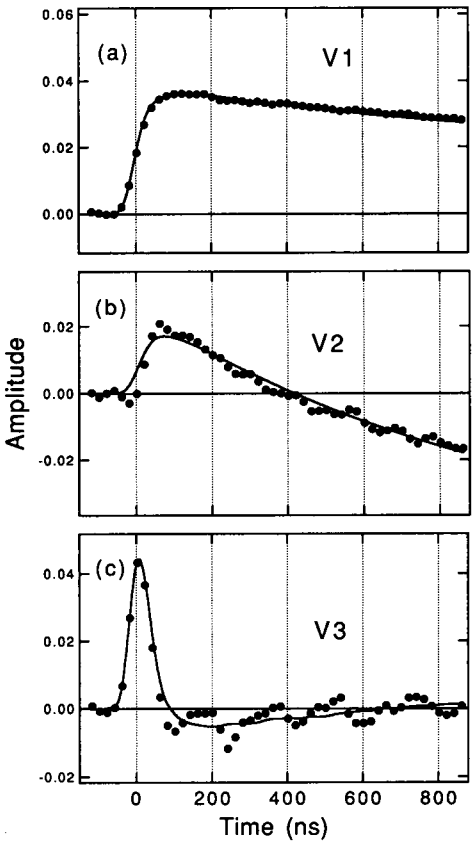

FIGURE 6 The best fits of V1 (*a*), V2 (*b*), and V3 (*c*) with a combination of $F_\infty(t)$, $F_{1000}(t)$, and $F_{10}(t)$ (——). *c* is identical with Fig. 4 *b*.

that could not be removed completely. Similar noise is still contained in V3, although to much less extent than the real signal. The other 45 U and V spectra (not shown) did not show any signals other than noise either. The weight factors of the first three base spectra were relatively larger than the other 47 (data not shown). It is clear, therefore, that the spectra shown in Fig. 2 can be expressed by these three time-dependent components, as expected.

The matrix is thus represented as:

$$A = U1 \times S1 \times V1 + U2 \times S2 \times V2 + U3 \times S3 \times V3. \quad (4)$$

Among the three changes, the first rise in the V vectors is the signal because of the delayed instrumental response. Therefore, there remain virtually only two components changing with different kinetics, and V1, V2, and V3 should be fitted with two exponential functions and a step function, which were convoluted with the IRF presented in Fig. 1. A rapidly decaying component is mainly manifested in V3 around time 0. Another kinetic change in V1 and V2 after 100 ns is well fitted with the time constant of 1 μs, and is in good agreement with the rate of the KL-to-L conversion that was observed previously under the identical sample conditions (Sasaki et al., 1993).

The fastest kinetic change in V3 is comparable with the present instrumental response, indicating that the process occurs much faster than 60 ns, FWHM of IRF. It should be noted that, in the 1000~900 cm^{-1} region, the characteristic band at 956 cm^{-1} in U3 is different from that in U1 (984 cm^{-1}) (Fig. 4). To estimate the time constant of the fast process, we then attempted to fit V3 with exponential functions convoluted with the IRF, $F_5(t)$, $F_{10}(t)$, and $F_{20}(t)$ shown in Fig. 1, respectively.

Fig. 5 shows the results of the fit of V3 with each of these functions in combination with $F_{1000}(t)$ and $F_\infty(t)$ (*solid lines*). The V3 vector with an increased number of points around time 0 obtained by averaging two spectra (*open squares*) in addition to 10 spectra (*filled squares*) are also depicted in Fig. 4 *a–c* to evaluate the fit more precisely. Fits with either $F_5(t)$ (Fig. 5 *a*) or $F_{10}(t)$ (Fig. 5 *b*) are much better than that with $F_{20}(t)$ (Fig. 5 *c*), which deviates noticeably. Therefore, it can be concluded that a conversion other than the KL-to-L conversion (1000 ns) takes place with the time constant below 20 ns. However, the systematic noise contained in V3 precluded us from distinguishing further the difference between the 5- and 10-ns fits only in shape. We therefore considered another

factor. Because the amplitude of $F_5(t)$ is about two-thirds as large as $F_{10}(t)$ (Fig. 1), the spectral amplitude of the rapidly changing component constructed as the consequence of the 5-ns fit became extremely large as compared with the other components, whereas that obtained as the result of 10-ns fit showed more reasonable size (see Fig. 7). We therefore adopted the 10-ns fit rather than the 5-ns fit, even though the latter seems to be more coincident with V3. A possible reason for the deviation from 10-ns fit is that the overlapped systematic noise in V3 could not be removed completely by subtracting the noise recorded by inserting the shutter between the laser and the sample.

V1 and V2 were also nicely fitted with a combination of $F_{10}(t)$, $F_{1000}(t)$, and $F_\infty(t)$ as shown in Fig. 6. The matrix A is then expressed by the linear combination of the fitted curves in place of V vectors as follows:

$$A = \Sigma Ui \times Si \times Vi = \Sigma Ui \times Si \times [ai \times F_{10}(t) + bi \times F_{1000}(t) + ci \times F_\infty(t)] \quad (i = 1, 2, \text{and } 3), \quad (5)$$

where

$$\begin{array}{lll} a1 = 0.02 & b1 = -0.02 & c1 = 0.019 \\ a2 = -0.02 & b2 = 0.072 & c2 = 0.048 \\ a3 = 0.35 & b3 = -0.018 & c3 = 0.0087 \end{array} \quad (6)$$

As are seen in the above parameters, the 10-ns component is dominant (~88%) in V3, whereas the slower and constant components contribute considerably in V1 and V2.

Using these parameters multiplied to the convoluted functions, the spectral components corresponding to each of the kinetics of convoluted functions are calculated as follows:

$$\begin{aligned} A &= \Sigma Ui \times Si \times ai \times F_{10}(t) + \Sigma Ui \times Si \times bi \times F_{1000}(t) \\ &\quad + \Sigma Ui \times Si \times ci \times F_\infty(t) \quad (i = 1, 2, \text{and } 3) \\ &= B(10\text{ ns}) \times F_{10}(t) + B(1000\text{ ns}) \times F_{1000}(t) \\ &\quad + B(\text{infinite}) \times F_\infty(t) \end{aligned} \quad (7)$$

where B(10 ns), B(1000 ns), and B(infinite) represent spectra attributed to the kinetics with the time constant of 10 ns, 1000 ns, and infinite, respectively. B(infinite) should be attributed to the difference spectrum of L vs. BR (the L-BR spectrum), because the decay rate constant of L (~40 μs) is essentially infinite in this time range. B(1000 ns) is then attributable to the KL-L spectrum in view of Sasaki et al. (1993). B(10 ns) shows that there is an additional component that decays with time constant of 10 ns. We assign this component to K according to the visible spectroscopy by Shichida et al. (1983) and Milder and Kliger (1988), who discriminated between the spectra in the picosecond and nanosecond time domains.

Based on the result that there are two changing processes with different time constants, there are three possible kinetic models. In the sequential model where K converts to KL, B(10 ns) is attributed to the K-KL spectrum. The second model is the parallel conversion of both K and KL to L in 10 and 1000 ns, respectively. In this case, B(10 ns) is attributed to the K-L spectrum. The third is another parallel model in which K decays back to BR and KL decays to L. However, this model is excluded because B(10 ns), which is attributed to K-BR spectrum in this case, does not show any changes due to 13-*cis* to all-*trans* isomerization in the fingerprint region (1300~1100 cm^{-1}) (data not shown).

The difference spectrum of KL-BR is calculated as:

$$\begin{aligned} KL\text{-}BR &= KL\text{-}L + L\text{-}BR \\ &= B(1000\text{ ns}) + B(\text{infinite}). \end{aligned} \quad (8)$$

K-BR spectrum is calculated similarly but is model-dependent. In the sequential model where K changes into KL, it is calculated according to:

$$\begin{aligned} K\text{-}BR^{seq} &= K\text{-}KL + KL\text{-}BR = B(10\text{ ns}) + B(\text{infinite}) \\ &\quad + B(1000\text{ ns}). \end{aligned} \quad (9)$$

In the parallel model where K changes into L, it is calculated according to:

$$\begin{aligned} K\text{-}BR^{par} &= K\text{-}L + L\text{-}BR \\ &= B(10\text{ ns}) + B(\text{infinite}). \end{aligned} \quad (10)$$

Fig. 7 *a* shows the difference spectra of K-BR^{seq} (*a*), K-BR^{par} (*b*), KL-BR (*c*), and L-BR (*d*) thus obtained. The spectral shapes of KL-BR and L-BR are in good agreement with those observed previously (Sasaki et al., 1993). The

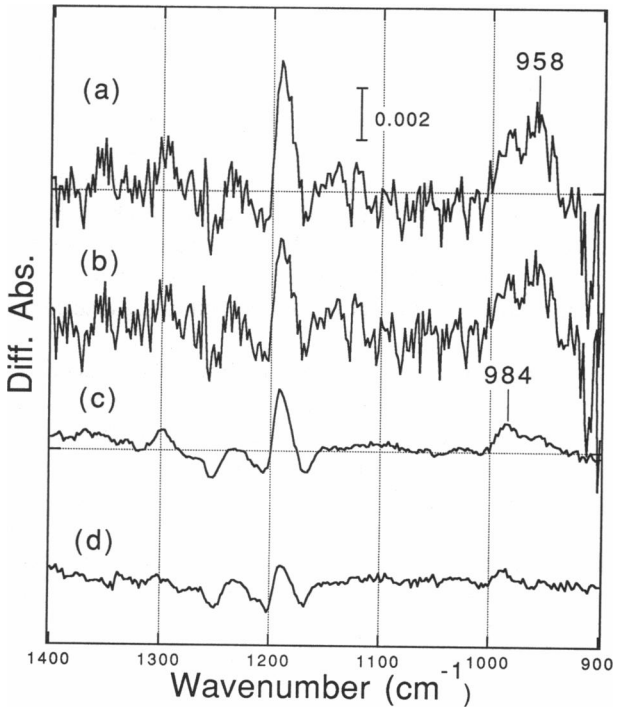

FIGURE 7 The calculated difference spectra of intermediates with time constants of 10 ns, 1000 ns, and infinite (>1000 ns) versus BR. (*a*) K^{seq}-BR, (*b*) K^{par}-BR, (*c*) KL-BR, and (*d*) L-BR difference spectra. K^{seq} and K^{par} are the intermediate with time constant of 10 ns calculated on the basis of sequential and parallel schemes, respectively. KL is the intermediate with time constant of 1000 ns. L is the intermediate with time constant of infinite.

HOOP band at 984 cm^{-1} seen in the L-BR spectrum is due to the coexistence of KL with L because of a back-reaction of L to KL (Váró and Lanyi, 1991; Sasaki et al., 1993). The K-BR spectra in the both sequential (*a*) and parallel (*b*) models look almost identical to each other except that the spectral intensities are smaller in the parallel model. The K-BR spectrum has a different feature from that of KL-BR in the HOOP region (below 1000 cm^{-1}). K has the HOOP band at 958 cm^{-1}, whereas KL has the HOOP band at 984 cm^{-1}. The spectra >1000 cm^{-1} appear to be similar to each other.

DISCUSSION

In our previous experiment (Sasaki et al., 1993), which presented the spectra in every 200-ns step, we detected the conversion of KL-to-L and showed its time constant to be ~1 μs. Even with this time resolution, we could detect a small change in the HOOP region between the spectra before and after 200 ns; The 958 cm^{-1} band in the first two spectra exhibited a larger intensity than in the later spectra. We suggested that this change was the K-to-KL conversion.

In low temperature FTIR spectroscopic studies, K^{LT} is produced by irradiation of BR at 77 K (Rothschild and Marrero, 1982; Siebert and Mäntele, 1983). Rothschild et al. (1985) found another K species at 135 K to be a mixture with K^{LT}. Interestingly, the spectral shape of KL looked similar to the K-like species (Sasaki et al., 1993). We therefore suggested that K would be attributable to K^{LT}, which had the strongest HOOP band at 958 cm^{-1}.

Heterogeneity of the K intermediate at 90 K was observed by Balashov et al. (1991) in visible absorption spectroscopy by deconvoluting the kinetic curve upon photoconversion of K to BR into three exponentials. However, any one of these components is not attributable to the K-like species at 135 K, because the K-BR FTIR spectrum at equivalent temperature does not show any typical bands due to the K-like species at 135 K. These components might arise from three different conformations of BR that are stable at 90 K, but are in equilibrium with each other at higher temperatures, as the authors discussed.

In the present study, we measured the infrared spectra of the conversion processes of BR in the −120~860-ns time range after excitation with a laser pulse with 5-ns width. Taking the IRF into consideration, the kinetic profiles of the spectra were analyzed by SVD and fitted with two convoluted exponential functions and one convoluted step function. As a result, 10- and 1000-ns changing components and a constant component were extracted. The conversion of 10 ns may correspond to the K-to-KL conversion proposed previously on evidence obtained by visible spectroscopy in a similar time range (Shichida et al., 1983; Milder and Kliger, 1988).

Yamamoto et al. (1994), however, recently reported a series of visible spectra in a wide time region between 500 ps and 3.5 μs without changing their instrument and optical geometry of the sample cell. Their data showed no spectral transition corresponding to the K-to-KL conversion. They suggested that the slight red-shift of the K detected by previous picosecond spectroscopy relative to that observed by nanosecond system could have originated from spectral narrowing by thermal relaxation of the intermediate, although they did not exclude the possibility of heterogeneity of the K species.

In this view, the conversion of 10 ns detected by our infrared spectroscopy might not correspond to the same K-to-KL conversion as observed by the earlier visible spectroscopy (Shichida et al., 1983; Milder and Kliger, 1988). Nevertheless, we reserve the name of K and KL for the two K species that are dominant in picosecond and nanosecond time domains, respectively, so as to clearly distinguish between them.

The 10-ns conversion process corresponds to the decaying process of K. There are two possibilities regarding the scheme, the sequential model in which K converts to KL and the parallel model in which K decays directly to L. In the latter case, a noticeable amount of L should appear in the early nanosecond time domain (<100 ns). However, in the data of Sasaki et al. (1993), we did not notice any bands because of perturbations of Asp-96 and Asp-115 specific for L up to 600 ns. For this reason, we consider the sequential model to be more likely.

In both models, the spectra of K and KL show remarkable differences in the HOOP region. The 958 cm^{-1} band is prominent in K, whereas the 984 cm^{-1} band predominates in KL. Because such a considerable shift of the band cannot occur through the thermal relaxation described by Yamamoto et al. (1994), it reveals the existence of two K-like species, K and KL. This is supported by the evidence that intermediates similar to K and KL are trapped by low temperature infrared spectroscopy (Rothschild et al., 1985; Sasaki et al., 1993). At 135 K, illumination of BR with green light (500 nm) produces two types of K species; one that has absorption band to the longer wavelength side was reverted to BR by illumination with 700-nm light, whereas the other was reverted by illumination with >630-nm light. The former is identical with K^{LT}, which can be produced by illumination of BR with green light at 77 K and the latter was called the K-like species. Most spectral features, especially the HOOP bands of K^{LT} and the K-like species, correspond well to those of the K and KL intermediates in the present time-resolved study, respectively.

The 958 cm^{-1} band of K appears at the same frequency in K^{LT}. The corresponding band in K^{LT} is mainly composed of the C_{15}-HOOP mode (Maeda et al., 1991). The 984 cm^{-1} band of KL was also assigned to the same vibrational mode (Weidlich and Siebert, 1993). Because the appearance of the strong HOOP bands in an infrared spectrum as well as a Raman spectrum originates from a distorted conformation of the chromophore (Fahmy et al., 1989), we suggest that the K and KL differ in a chromophore twist around the 15 position, that is, a twist around the C_{14}-C_{15} bond. In the sequential model, the Schiff base rotates around the C_{14}-C_{15} bond in the conversion of K to L through KL, leading to a distorted chromophore structure in L (Maeda et al., 1994).

This could be the 13,14-dicis form proposed by Zhou et al. (1993). This model would explain the following matters. The red-shifted absorption spectra of K and KL might be caused by the photoisomerization of the chromophore to 13-*cis*, which separates the Schiff base proton from the counterion, Asp-85. The blue-shifted spectrum in L could result when the Schiff base proton approaches the same counterion again in L by twisting of the C_{14}-C_{15} bond. Such a conformation would also be suitable for transfer of the Schiff base proton to Asp-85 in the next step that leads to M.

An alternative possibility for the K-to-KL conversion is that it is a process for relaxing a distorted structure around the 15 position in K to the planar 13-*cis* chromophore in L, on the basis of an observation of resonance Raman experiments that the chromophore in L assumes 14-*trans*. (Fodor et al., 1988). In this case, the distortion in the chromophore in K and KL is transmitted to the protein in L to restore the interaction between the Schiff base proton and Asp-85.

The K-to-KL and KL-to-L conversions are steps in which energy stored in the distorted chromophore is transferred to the protein, as were observed in the perturbations of vibrational bands in L for Asp-96, Asp-115 (Braiman et al., 1988a; Maeda et al., 1992a), Trp-182 (Yamazaki et al., 1995), and water molecules (Maeda et al., 1992b).

A more detailed investigation on K and KL will be implemented by use of mutant proteins in which an amino acid residue around the Schiff base is replaced by other residues. For instance, the photoproduct of Tyr-57 → Phe at 77 K looks more similar to KL than K (Braiman et al., 1988b), indicating that Tyr-57 contributes to stabilizing K. Similar observations are obtained also with Thr-89 → Ala (Rothschild et al., 1992), and Arg-82 → Ala (our unpublished data) in which both K and KL are produced by irradiation at 77 K. It would be worthwhile to investigate the structure of K and KL using these mutants not only for the precise understanding of these intermediates but also for the elucidation of the chromophore conformation as well as protein structure in L, which is a key intermediate for carrying out proton transfer in the next L-to-M conversion.

This work is partly supported by a grant-in-Aid for scientific research to A. Maeda (06404082, 06044123, and 05259212) and by Encouragement of Young Scientist to H. Kandori (06780545) from the Japanese Ministry of Education, Science and Culture, and to J. Sasaki by Research Fellowships of the Japanese Society for the Promotion of Science for Young Scientist.

REFERENCES

Balashov, S. P., N. V. Karneyeva, F. F. Litvin, and T. G. Ebrey. 1991. Bathoproducts and conformations of all-*trans*- and 13-*cis*-bacteriorhodopsin at 90 K. *Photochem. Photobiol.* 54:949–953.

Braiman, M. S., T. Mogi, T. Marti, L. J. Stern, H. G. Khorana, and K. J. Rothschild. 1988a. Vibrational spectroscopy of bacteriorhodopsin mutants: light-driven proton transport involves protonation change of aspartic acid residues 85, 96, and 212. *Biochemistry.* 27:8516–8520.

Braiman, M. S., T. Mogi, L. J. Stern, N. R. Hackett, B. H. Chao, H. G. Khorana, and K. J. Rothschild. 1988b. Vibrational spectroscopy of bacteriorhodopsin mutants. I. Tyrosine-185 protonates and deprotonates during the photocycle. *Proteins Struct. Funct. Genet.* 3:219–229.

Diller, R., M. Iannone, B. R. Cowen, S. Maiti, R. A. Bogomolni, and R. M. Hochstrasser. 1992. Picosecond dynamics of bacteriorhodopsin, probed by time-resolved infrared spectroscopy. *Biochemistry.* 31:5567–5572.

Dobler, J., W. Zinth, W. Kaiser, and D. Oesterhelt. 1988. Excited-state reaction dynamics of bacteriorhodopsin studies by femtosecond spectroscopy. *Chem. Phys. Lett.* 144:215–220.

Doig, S. J., P. J. Reid, and R. A. Mathies. 1991. Picosecond time-resolved resonance Raman spectroscopy of bacteriorhodopsin's J, K, and KL intermediates. *J. Phys. Chem.* 95:6372–6379.

Fahmy, K., F. Siebert, M. F. Grossjean, and P. Tavan. 1989. The photoisomerization in bacteriorhodopsin studied by FTIR linear dichroism and photoselection experiments combined with quantum mechanical theoretical analysis. *J. Mol. Struct.* 214:257–288.

Fodor, S. P. A., W. T. Pollard, R. Gebhard, E. M. M. van den Berg, J. Lugtenburg, and R. A. Mathies. 1988. Bacteriorhodopsin's L550 intermediate contains a C14-C15 s-*trans*-retinal chromophore. *Proc. Natl. Acad. Sci. USA.* 85:2156–2160.

Govindjee, R., S. P. Balashov, and T. G. Ebrey. 1990. Quantum efficiency of the photochemical cycle of bacteriorhodopsin. *Biophys. J.* 58:597–608.

Kandori, H., K. Yoshihara, H. Tomioka, H. Sasabe, and Y. Shichida. 1993. Comparative study of primary photochemical events of two retinal proteins, bacteriorhodopsin and halorhodopsin, by use of subpicosecond time-resolved spectroscopy. *Chem. Phys. Lett.* 211:385–391.

Lanyi, J. K. 1993. Proton translocation mechanism and energetics in the light-driven pump bacteriorhodopsin. *Biochim. Biophys. Acta.* 1183: 241–261.

Lozier, R. H., R. A. Bogomolni, and W. Stoeckenius. 1975. Bacteriorhodopsin: a light-driven proton pump in *Halobacterium halobium*. *Biophys. J.* 15:955–962.

Maeda, A., J. Sasaki, J.-M. Pfefferlé, Y. Shichida, and T. Yoshizawa. 1991. Fourier transform infrared spectral studies on the Schiff base mode of all-*trans* bacteriorhodopsin and its photointermediates, K and L. *Photochem. Photobiol.* 54:911–921.

Maeda, A., J. Sasaki, Y. Shichida, T. Yoshizawa, M. Chang, B. Ni, R. Needleman, and J. K. Lanyi. 1992a. Structures of aspartic acid-96 in the L and N intermediates of bacteriorhodopsin: analysis by Fourier transform infrared spectroscopy. *Biochemistry.* 31:4684–4690.

Maeda, A., J. Sasaki, Y. Shichida, and T. Yoshizawa. 1992b. Water structural change in the bacteriorhodopsin photocycle: analysis by Fourier transform infrared spectroscopy. *Biochemistry.* 31:463–467.

Maeda, A., J. Sasaki, Y. Yamazaki, R. Needleman, and J. K. Lanyi. 1994. Interaction of Asparate-85 with a water molecule and the protonated Schiff base in the L intermediate of bacteriorhodopsin: a Fourier transform infrared spectroscopic study. *Biochemistry.* 33:1713–1717.

Mathies, R. A., C. H. B. Cruz, W. T. Pollard, and C. V. Shank. 1988. Direct observation of the femtosecond excited-state *cis-trans* isomerization in bacteriorhodopsin. *Science.* 240:777–779.

Mathies, R. A., S. W. Lin, J. B. Ames, and W. T. Pollard. 1991. From femtosecond to biology: mechanism of bacteriorhodopsin's light-driven proton pump. *Annu. Rev. Biophys. Biophys. Chem.* 20:491–518.

Milder, S. J., and D. S. Kliger. 1988. A time-resolved spectral study of the L and KL intermediate of bacteriorhodopsin. *Biophys. J.* 53:465–468.

Oesterhelt, D., and W. Stoeckenius. 1974. Isolation of the cell membrane of Halobacterium halobium and its fraction into red and purple membrane. *Methods Enzymol.* 31:667–678.

Rothschild, K. J., and H. Marrero. 1982. Infrared evidence that the Schiff base of bacteriorhodopsin is protonated: bR570 and K intermediate. *Proc. Natl. Acad. Sci. USA.* 79:4045–4049.

Rothschild, K. J., Y.-W. He, S. Sonar, T. Marti, and H. G. Khorana. 1992. Vibrational spectroscopy of bacteriorhodopsin mutants. *J. Biol. Chem.* 267:1615–1622.

Rothschild, K. J., P. Roepe, and J. Gillespie. 1985. Fourier transform infrared spectroscopic evidence for the existence of two conformations of the bacteriorhodopsin primary photoproduct at low temperature. *Biochim. Biophys. Acta.* 808:140–148.

Sasaki, J., A. Maeda, C. Kato, and H. Hamaguchi. 1993. Time-resolved infrared spectral analysis of the KL-to-L conversion in the photocycle of bacteriorhodopsin. *Biochemistry.* 32:867–871.

Shichida, Y., S. Matuoka, Y. Hidaka, and T. Yoshizawa. 1983. Absorption spectra of intermediates of bacteriorhodopsin measured by laser photolysis at room temperatures. *Biochim. Biophys. Acta.* 723:240–246.

Siebert, F., and W. Mäntele. 1983. Investigation of the primary photochemistry of bacteriorhodopsin by low temperature Fourier-transform infrared spectroscopy. *Eur. J. Biochem.* 130:565–573.

Stoeckenius, W., and R. H. Lozier. 1974. Light energy conversion in *Halobacterium halobium*. *J. Supramol. Struct.* 2:769–744.

Tokunaga, F., T. Iwasa, and T. Yoshizawa. 1976. Photochemical reaction of bacteriorhodopsin. *FEBS Lett.* 72:33–38.

Váró, G., and J. K. Lanyi. 1991. Thermodynamics and energy coupling in the bacteriorhodopsin photocycle. *Biochemistry.* 30:5016–5022.

Weidlich, O., and F. Siebert. 1993. Time-resolved step-scan FT-IR investigations of the transition from KL to L in the bacteriorhodopsin photocycle: identification of chromophore twists by assigning hydrogen-out-of-plane (HOOP) bending vibrations. *Appl. Spectrosc.* 47: 1394–1400.

Yamamoto, N., T. W. Ebbesen, and H. Ohtani. 1994. Does the KL intermediate exist in the photocycle of bacteriorhodopsin? *Chem. Phys. Lett.* 228:61–65.

Yamazaki, Y., J. Sasaki, M. Hatanaka, H. Kandori, A. Maeda, R. Needleman, T. Shinada, K. Yoshihara, L. S. Brown, and J. K. Lanyi. 1995. Interaction of tryptophan-182 with the retinal 9-methyl group in the L intermediate of bacteriorhodopsin. *Biochemistry.* 34:577–582.

Yuzawa, T., C. Kato, M. W. George, and H. Hamaguchi. 1994. Nanosecond time-resolved infrared spectroscopy with a dispersive scanning spectrometer. *Appl. Spectrosc.* 46:684–690.

Zhou, F., A. Windemuth, and K. Schulten. 1993. Molecular dynamics study of the proton pump cycle of bacteriorhodopsin. *Biochemistry.* 32:2291–2306.